Fully programmable two-dimensional pulse shaper for broadband line-by-line amplitude and phase control

Andrew J. Metcalf,[1,*] Victor Torres-Company,[1,2] V.R. Supradeepa,[1,3]
Daniel E. Leaird,[1] and Andrew M. Weiner[1]

[1]*Department of Electrical and Computer Engineering, Purdue University, 465 Northwestern Avenue, West Lafayette, IN 47906, USA*
[2]*Currently with the Microtechnology and Nanoscience Department, Chalmers University of Technology, Gothenburg, Sweden*
[3]*Currently with OFS Laboratories, New Jersey, USA*
[*]*metcalfa@purdue.edu*

Abstract: We introduce a fully programmable two-dimensional (2D) pulse shaper, able to simultaneously control the amplitude and phase of very fine spectral components over a broad bandwidth. This is achieved by aligning two types of spectral dispersers in a cross dispersion setup: a virtually imaged phased array for accessing fine resolution and a transmission grating for achieving broad bandwidth. We take advantage of the resultant 2D dispersion profile as well as introduce programmability by adding a 2D liquid crystal on silicon spatial light modulator at the masking plane. Our shaper has a resolution of ~3 GHz operating over the entire 'C' band of >5.8 THz. Experimental evidence is provided that highlights the full programmability, fine spectral control, and broad bandwidth operation (limited currently by the bandwidth of the input light). We also show line-by-line manipulation of record 836 comb lines over the C-band.

©2013 Optical Society of America

OCIS codes: (320.0320) Ultrafast optics; (320.5540) Pulse shaping.

References and links

1. A. M. Weiner, "Ultrafast optical pulse shaping: a tutorial review," Opt. Commun. **284**(15), 3669–3692 (2011).
2. A. M. Weiner, "Femtosecond pulse shaping using spatial light modulators," Rev. Sci. Instrum. **71**(5), 1929–1960 (2000).
3. J. P. Heritage and A. M. Weiner, "Advances in spectral optical code-division multiple-access communications," IEEE J. Sel. Top. Quantum Electron. **13**(5), 1351–1369 (2007).
4. N. Dudovich, D. Oron, and Y. Silberberg, "Single-pulse coherently controlled nonlinear Raman spectroscopy and microscopy," Nature **418**(6897), 512–514 (2002).
5. A. M. Weiner, D. E. Leaird, G. P. Wiederrecht, and K. A. Nelson, "Femtosecond pulse sequences used for optical manipulation of molecular motion," Science **247**(4948), 1317–1319 (1990).
6. T. Brixner, N. H. Damrauer, P. Niklaus, and G. Gerber, "Photoselective adaptive femtosecond quantum control in the liquid phase," Nature **414**(6859), 57–60 (2001).
7. S. T. Cundiff and A. M. Weiner, "Optical arbitrary waveform generation," Nat. Photonics **4**(11), 760–766 (2010).
8. J. T. Willits, A. M. Weiner, and S. T. Cundiff, "Line-by-line pulse shaping with spectral resolution below 890 MHz," Opt. Express **20**(3), 3110–3117 (2012).
9. V. R. Supradeepa, C.-B. Huang, D. E. Leaird, and A. M. Weiner, "Femtosecond pulse shaping in two dimensions: towards higher complexity optical waveforms," Opt. Express **16**(16), 11878–11887 (2008).
10. M. Shirasaki, "Large angular dispersion by a virtually imaged phased array and its application to a wavelength demultiplexer," Opt. Lett. **21**(5), 366–368 (1996).
11. S. J. Xiao and A. M. Weiner, "2-D wavelength demultiplexer with potential for >= 1000 channels in the C-band," Opt. Express **12**(13), 2895–2902 (2004).
12. S. A. Diddams, L. Hollberg, and V. Mbele, "Molecular fingerprinting with the resolved modes of a femtosecond laser frequency comb," Nature **445**(7128), 627–630 (2007).
13. T. Chan, E. Myslivets, and J. E. Ford, "2-dimensional beamsteering using dispersive deflectors and wavelength tuning," Opt. Express **16**(19), 14617–14628 (2008).

14. T. K. Chan, J. Karp, R. Jiang, N. Alic, S. Radic, C. F. Marki, and J. E. Ford, "1092 channel 2-D array demultiplexer for ultralarge data bandwidth," J. Lightwave Technol. **25**(3), 719–725 (2007).
15. V. R. Supradeepa, D. E. Leaird, and A. M. Weiner, "A 2-D VIPA-grating pulse shaper with a liquid crystal on silicon (LCOS) spatial light modulator for broadband, high resolution, programmable amplitude and phase control," in Proceedings of Ultrafast Phenomena XVII, 811–813 (2010).
16. A. J. Metcalf, V. Torres-Company, V. R. Supradeepa, D. E. Leaird, and A. M. Weiner, Programmable broadband ultra-fine resolution 2-D pulse shpaing," in XVIIIth International conference on Ultrafast phenomena, Vol. 41 of EPJ Web of Conferences (EJP Web of Conferences, 2013).
17. M. S. Kirchner and S. A. Diddams, "Grism-based pulse shaper for line-by-line control of more than 600 optical frequency comb lines," Opt. Lett. **35**(19), 3264–3266 (2010).
18. V. R. Supradeepa, E. Hamidi, D. E. Leaird, and A. M. Weiner, "New aspects of temporal dispersion in high-resolution Fourier pulse shaping: a quantitative description with virtually imaged phased array pulse shapers," J. Opt. Soc. Am. B **27**(9), 1833–1844 (2010).
19. J. C. Vaughan, T. Hornung, T. Feurer, and K. A. Nelson, "Diffraction-based femtosecond pulse shaping with a two-dimensional spatial light modulator," Opt. Lett. **30**(3), 323–325 (2005).
20. E. Frumker and Y. Silberberg, "Phase and amplitude pulse shaping with two-dimensional phase-only spatial light modulators," J. Opt. Soc. Am. B **24**(12), 2940–2947 (2007).
21. A. J. Metcalf, V. Torres-Company, D. E. Leaird, and A. M. Weiner, "High-power broadly tunable electro-optic frequency comb generator," IEEE J. Sel. Top. Quantum Electron. **19**(6), 3500306 (2013), doi:10.1109/JSTQE.2013.2268384.
22. S. J. Xiao, A. M. Weiner, and C. Lin, "A dispersion law for virtually imaged phased-array spectral dispersers based on paraxial wave theory," IEEE J. Quantum Electron. **40**(4), 420–426 (2004).
23. A. J. Metcalf, "Programmable two-dimensional ultra-complex broadband fine-resolution pulse shaping," MSECE thesis (Purdue University, 2012). *http://guides.lib.purdue.edu/dissertations*.
24. Z. Jiang, C.-B. Huang, D. E. Leaird, and A. M. Weiner, "Optical arbitrary waveform processing of more than 100 spectral comb lines," Nat. Photonics **1**(8), 463–467 (2007).
25. J. Caraquitena, Z. Jiang, D. E. Leaird, and A. M. Weiner, "Tunable pulse repetition-rate multiplication using phase-only line-by-line pulse shaping," Opt. Lett. **32**(6), 716–718 (2007).
26. V. Torres-Company, A. J. Metcalf, D. E. Leaird, and A. M. Weiner, "Multichannel radio-frequency arbitrary waveform generation based on multiwavelength comb switching and 2-D line-by-line pulse shaping," IEEE Photon. Technol. Lett. **24**(11), 891–893 (2012).

1. Introduction

Optical pulse shaping is a widely adopted method to reshape ultrafast light pulses through the complex manipulation of their optical spectrum [1, 2]. It is used in numerous applications ranging from optical communications to coherent quantum control [3–6]. Also, with recent advances in GHz class frequency combs, a new application termed optical arbitrary waveform generation (OAWG) has developed, which requires control of individual components of the frequency comb [7]. This 'line-by-line' manipulation allows for generation of 100% duty factor waveforms, which cannot be accomplished by controlling groups of lines together. These applications can also benefit from the shaper's ability to simultaneously operate over a broad bandwidth, as is needed when dealing with ultrashort pulses. However, conventional pulse shapers are limited by an inherent trade-off: typical spectral dispersers either have broad bandwidth operation with coarse spectral control or fine spectral control with a limited bandwidth. For example, the current spectral resolution record for line-by-line shaping is 890 MHz, however, comb lines could only be arbitrarily controlled over a limited bandwidth of 25 GHz (or ~28 total lines) [8].

To achieve fine spectral control over a broad bandwidth, our group designed a 2D shaper that combines a fine resolution disperser with a broadband one, aligned in a cross dispersion setup [9]. A modified Fabry-Perot etalon called a virtually imaged phased array (VIPA) acts as a hyper-fine spectral disperser [10]. However, a VIPA, like any Fabry-Perot device, is limited by its free spectral range (FSR), which is usually at most a few hundred GHz. This means that any frequency that is separated by an integer multiple of the FSR is dispersed to an identical spatial location. To break up this spatial redundancy, the vertically displaced VIPA light is sent through a transmission grating which spreads the VIPA FSRs along the horizontal axis, resulting in a 2D matrix of dispersed light while granting each wavelength an accessible spatial location [11, 12]. We reported initial results of our shaper design in [9], but were limited to using static fixed masks. Other efforts employing similar disperser

arrangements have been used for large channel number optical demultiplexing and wavelength-controlled laser scanning [13, 14]. In order to take full advantage of the 2D dispersion profile in our original geometry, we added a 2D liquid crystal on silicon (LCoS) spatial light modulator (SLM), which allows dynamic (~ms range) programmatic control of the shaper. We presented initial results using a 2D SLM in [15] and followed with preliminary results using the 2D SLM as a programmable device in [16]. Expanding on these initial proof-of-concept demonstrations, we now are able to achieve true programmatic control. By developing an automated wavelength-mapping and mask-creation algorithm, we allow a user to simply input a desired spectral shape and phase in a similar manner to commercially available shapers. With the added flexibility we can now push for increased complexity in the synthesized waveforms. In addition, a programmable device allows us to tackle issues such as controlling higher orders of VIPA light as well as addressing the highly nonlinear diffraction pattern inherent to this device, both of which help enhance the available extinction ratio.

In this contribution, we highlight this new programmatic control and its benefits. We start by briefly explaining our experimental setup. We then detail our wavelength-to-spatial-mapping procedure, a crucial piece in our ability to access and control finely spaced spectral features. Experimental evidence is then provided of simultaneous phase and amplitude shaping. In addition we highlight the broad bandwidth of the device through line-by-line spectral shaping of 836 lines across the C-Band. To our knowledge these are the most complex waveforms ever shaped in a line-by-line manner, increasing the number of discrete lines individually addressed by ~30% compared to that achieved in the experiments of [17], which were limited by the number of pixels (640) in the one dimensional SLM. In our experiment the number of lines is limited by the bandwidth of the optical pulse source; with a broader band source substantially more lines could be accommodated without changing the pulse shaper setup.

2. Experimental setup

The experimental setup is depicted in Fig. 1. Incident light passes a fiber circulator followed by a fiber polarization controller before being coupled to free space. A polarizer is then used to ensure the polarization state is aligned with that of the SLM. The polarized light is then focused into a thin window on the VIPA (Avanex Corp) by a cylindrical lens (f = 5 cm). The VIPA disperses light in the vertical direction, with angular redundancy for frequencies spaced by an integer number of its FSR (200 GHz). The vertically displaced light is then sent through a transmission grating (Wasatch Photonics) with a pitch of 940lines/mm that disperses the light horizontally, thus breaking up the spatial redundancy of the VIPA. Two cylindrical lenses, L2 (f = 15 cm) and L3 (f = 10 cm)are then required to focus the 2D matrix of dispersed light onto the masking plane in order to achieve the zero dispersion condition [18]. The modulated light from the SLM returns down the same path and gets output via the fiber circulator. In the absence of mask at the Fourier plane, the setup has been aligned so that the output spectrum and intensity cross-correlation are identical to the input, ensuring the dispersion-free condition [9].

The SLM is a Holoeye 1080p phase only LCoS device which is comprised of over two million pixels. To achieve simultaneous amplitude and phase shaping we form 'superpixels' that are made up by arranging 10 x 10 individual pixels together. Amplitude shaping is achieved by forming a finely spaced sawtooth phase grating within each superpixel, where the phase excursion of the grating determines the amount of power directed into higher order.
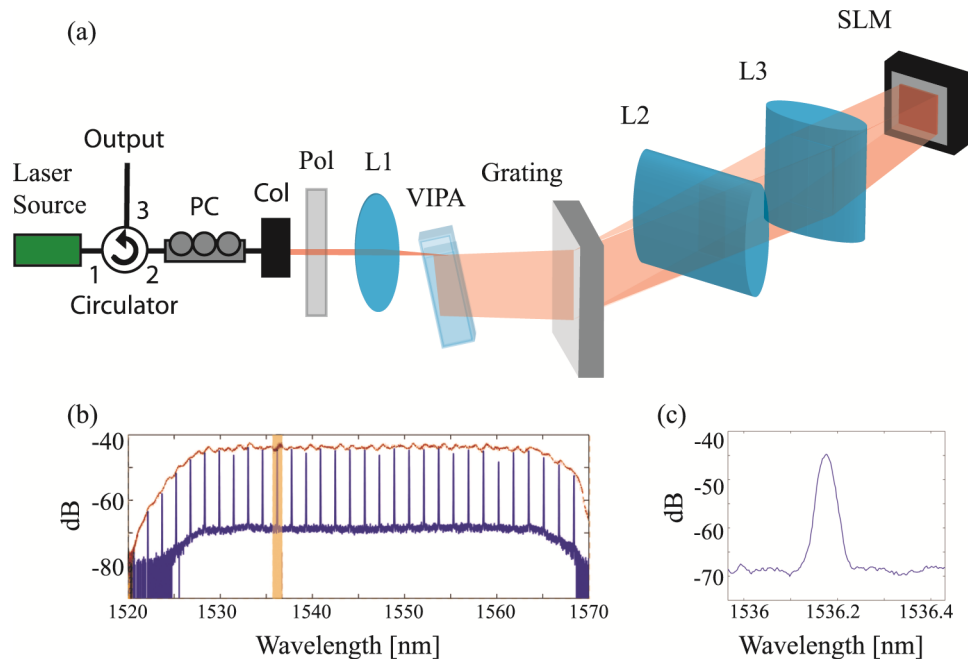
Fig. 1. (a) Shaper setup, (b) Output spectrum of shaper with no mask (red), Output spectrum of shaper with mask applied selecting one feature every 200 GHz, (c) zoom of feature from b.

Phase control is then achieved by changing the slowly varying the (average) phase level of the superpixel. Details of this method can be found in [19]. Our SLM surface has an 87% fill factor due to dead spaces between the individual pixels which contribute an amount of unmodulated light limiting the achievable extinction ratio. As demonstrated in [20] we can increase the extinction ratio by positioning the SLM slightly off axis and programming a grating pattern onto the SLM to direct only our modulated light into the return path. The extinction ratio is improved because now light we are unable to modulate is not coupled back. Figure 1(b) compares the output spectrum to the shaper (using an ASE source) with the output when a mask selecting one feature every 200 GHz is applied. Figure 1(c) is a zoomed trace of the highlighted feature in Fig. 1(b), showing an extinction ratio of ~20 dB, which we believe is limited by reflections in the setup. The narrowest line width of the feature achieved is ~3 GHz at −3 dB bandwidth over the entire optical span tested, comprising >5.8 THz. The ratio of optical span to (−3 dB) spectral resolution is nearly 2,000, which to our knowledge is the highest demonstrated in programmable pulse shaping. In the current configuration, the total loss of the shaper measured at the output of the circulator is ~18 dB, which is uniform across the full spectral range. For perspective, VIPA shapers alone typically have ~12 dB loss [9]; by adding a grating an additional 3 dB loss is added. On top of that, 3 dB loss is incurred when operating in the off-axis configuration described above. The majority of loss in our VIPA shaper is due to the inefficient coupling of light into the small slit on the VIPA face. If this can be optimized, the loss could be greatly diminished. In addition improving the fill factor of the SLM would negate the need to work in the 'off-axis' configuration which would allow us to regain an additional 3 dB without limiting the extinction ratio.

We use three types of light sources throughout our experimental demonstration. An Amplified Spontaneous Emission (ASE) source, with 40 nm bandwidth, is used in our wavelength-to-spatial mapping procedure and for some spectral shaping experiments. An electro-optically generated comb source with tunable repetition rate from 6 to 18 GHz is used to demonstrate line-by-line amplitude and phase shaping [21]. And finally, a spectrally

broadened electro-optic comb source is used to demonstrate the shaper's broad bandwidth capability.

3. Wavelength to spatial mapping

In order to achieve precise programmable control, a mapping technique relating the wavelength's spatial position vs. pixel location needs to be determined. This is an ambitious process in part due to the highly nonlinear dispersion characteristics of the VIPA, and in part due to the nontrivial intensity distribution of light diffraction by the VIPA into multiple orders. The tilt of the VIPA with respect to the incident light is what governs the amount of nonlinearity [22]; in an experimental setting this makes it difficult to predict an exact mask. Other efforts working with VIPA shapers and using fixed masks have ignored this nonlinearity [8, 9]. In addition, like other spectral dispersers based on diffraction, a VIPA diffracts a single wavelength into multiple orders. For a given wavelength the relative power in each order is governed by a Gaussian intensity envelope [22]. For an example see Fig. 2 (from [18]). The nonlinear wavelength spacing combined with the unique 2D dispersion profile means we cannot simply create fixed continuous masks. The goal of our mapping procedure is then to create a wavelength to pixel profile that has addressability much finer than the repetition rate of our source. We can then use this grid to define the center location of our superpixels.
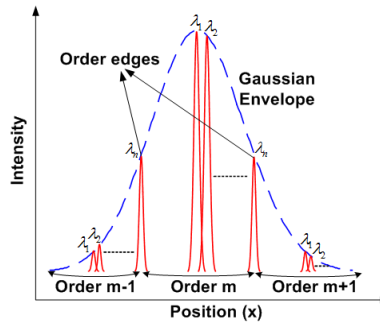

Fig. 2. VIPA's intensity distribution for a single FSR (from [18]).

Our procedure is as follows: Starting with the same shaper setup as detailed above, and using an ASE source which is flat across the C-band, the SLM is aligned so that reflected light will not couple into the return path. Then, by forming a superpixel with an appropriately defined phase grating we can direct a portion of light back into the return path. Recording the spectrum of the returned light will show a peak power at the wavelength associated with the superpixel location we turned on. However, to do this method for individual superpixels over the full 2 million pixel matrix would be very time consuming. To put some numbers to this, if we move our superpixel around the screen in steps of just 2 pixels and record data each time, it would require over 518,000 data acquisitions. We are able to decrease this number to only 1,500 data acquisitions by grouping superpixels together. Although this process still takes hours to complete (limited by the time it takes to get an OSA trace), it only needs to be completed once during the initial shaper alignment. After calibration, the shaper operates as a standalone device allowing for arbitrary mask creation over the full bandwidth with 0.6 GHz addressability. First, superpixels are joined together to form a row, then we iteratively move the row vertically down the screen, recording the spectrum each time. We then form a column of superpixels and move it horizontally, again recording the spectrum. Now through computer processing we multiply the row and column spectral power traces together to determine the corresponding wavelength at the intersecting superpixel location. The process is depicted in Fig. 3(a). The row traces (red) will intersect one frequency in each FSR, whereas the column traces (blue) will just select a portion of one FSR. When multiplied together, the spectrally

broader column traces act like a gate, selecting the correct spectral peak from the peaks in the row trace, Fig. 3(b). The width of the spectral features measured in a row trace define the resolution of the shaper (~3 GHz at −3 dB), whereas the addressability is given by the difference between two neighboring row traces (0.6 GHz) distinguished (red) and (green) in Fig. 3(a), 3(c). More detailed information on the mapping procedure can be found in [23]. After mapping we achieve a complete representation of both the power and wavelength at each spatial location on the SLM. For comparison, Fig. 3(d) shows an image taken with an IR camera of the Fourier plane power distribution. Figure 3(e) is a 2D plot of the recorded power distribution from the data collected from the mapping program, showing close comparison.

As mentioned above, it is our goal to control multiple orders of VIPA light. After our spatial mapping procedure is complete, we have a 2D grid of possible superpixel center points. Each point has a recorded wavelength and a reference power that is equal to the product of the row and column recorded powers. To determine the location of the main VIPA diffraction order we simply find the highest power location for a given wavelength; subsequent orders are found by searching for the next lowest power occurrence of the same wavelength. However, as noted above and depicted in Fig. 2, the intensity distribution between the various orders of VIPA diffracted light is dependent on the wavelength positions within the FSR. Wavelengths which fall in the center of the FSR have the majority of their power in the main VIPA diffraction order, whereas wavelengths which fall near the edge, have more power distributed to higher orders [18].
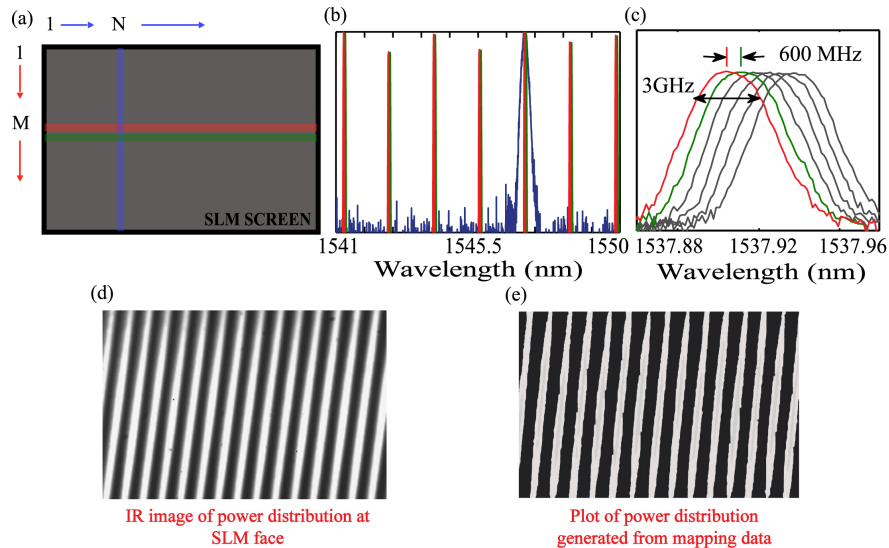

Fig. 3. (a) diagram of wavelength mapping procedure, column trace (blue), adjacent row traces (red and green), (b) power spectrum from row traces (red and green), power spectrum from column trace (blue), (c) power spectrum of adjacent row traces (red and green) (d) image taken of Fourier plane with an IR camera, (e) Plot of power distribution from mapping data

To highlight the importance of higher order control, we send a spectrally flat ASE light source to the shaper and compare the output spectrum when 1st, 2nd, and 3rd orders of VIPA light are controlled. First, we obtain a reference output spectrum by applying a generic flat-phase mask to the full SLM. It can be thought of as a giant superpixel the size of the SLM (1920 x 1080 pixels). Here, we say 'generic' because we have made no attempt to distinguish where the wavelengths are incident on the SLM; we basically set the SLM to act as a mirror and return all of the light. For the remaining masks, we use our mapping data to correctly position our superpixels, of size 10 x 10 pixels, to their correct spatial location on the SLM. For these masks, we only select a 12nm passband and set the rest of the spectrum to max

attenuation. In Fig. 4(b), we only locate and control the first diffraction order of the VIPA light. As expected, significant dips, which are periodic with the VIPA FSR (200GHz), are present in the output spectrum. Comparing to the theory, the peaks in the output spectrum correspond to wavelengths that landed in the center of a VIPA FSR, and therefore have most of their power concentrated in the 1st VIPA order. The dips then correspond to wavelengths which land near the edge of the VIPA FSR that have more of their power spread to higher diffraction orders. In Fig. 4(c) we locate and control an additional order of VIPA light, which we are referring to as '2nd Order'. We can see noticeable improvement in the flatness of the spectrum, but the dips are still visible. In Fig. 4(d), by locating and controlling a '3rd Order' of VIPA light, where the dips have almost completely vanished, and the output spectrum (red) matches our reference spectrum (blue).

We notice that there are still small (<1 dB) spectral ripples that are present at the output of the shaper, even when all light is returned, Fig. 4(a). These ripples most likely arise because of a deviation from the precise VIPA zero dispersion condition [18], which arises due to a slight shaper misalignment. If this dispersion condition is not completely satisfied, the shaper will introduce a small amount of temporal dispersion. In the case of multiple VIPA orders, the resulting relative phase difference between different orders of a given frequency will manifest itself as a spectral ripple [18]. This effect could conceivably be negated by applying different phases to the higher order light; however that is not attempted here.
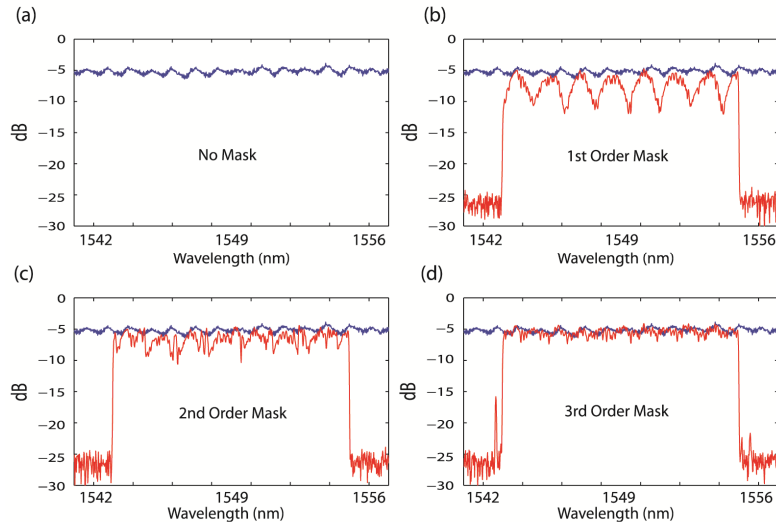

Fig. 4. Output spectrum of shaper with flat ASE source applied, (a) output when a generic mask is applied returning all light that is incident on the SLM, (b) Output spectrum when a mask is created returning only the light in the first VIPA diffraction order, (c) output spectrum when 2 VIPA orders are returned, (d) Output spectrum when 3 VIPA orders are returned.
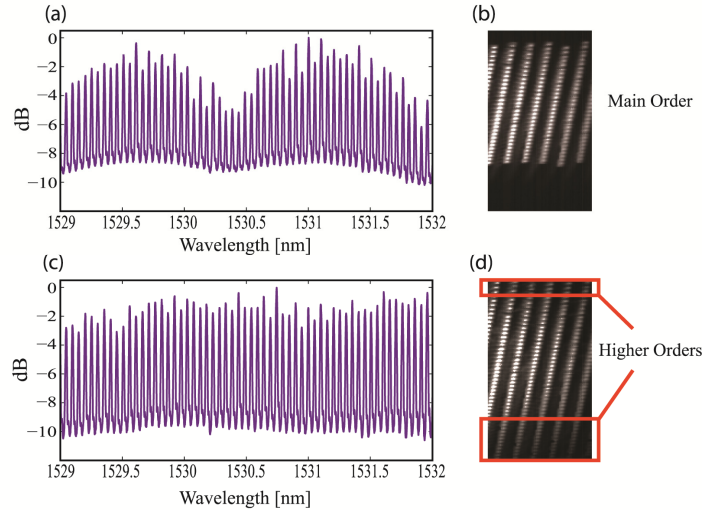
Fig. 5. (a) Shaper output with a 1st-order mask applied, (b) IR image of the Fourier plane showing the location of the 1st order light, (c) Shaper output with a 2nd-order mask applied, (d) IR image of the Fourier plane showing the location of 1st and 2nd orders of light.

An additional consideration is the spatial location of these higher orders, i.e. we require all of the higher orders to fall to unique locations on the SLM. According to the expected spatial distribution shown in Fig. 2, and with the VIPA diffraction occurring in the vertical dimension, we would expect the higher VIPA orders to occur above and below the main order of light, respectively. To verify the spatial location of the higher orders, we place a beam splitter in front of the SLM to allow imaging of the actual power distribution at the Fourier plane. In this example, a portion of a 6.5 GHz repetition rate, spectrally broadened frequency comb source is used. The discrete nature of the source allows us to distinguish the individual comb channels in our image. Figure 5(a) shows a portion of the output spectrum when only the first order of light is controlled; once again we see clear dips that are periodic with the VIPA FSR. The corresponding IR image of the power distribution on the SLM plane is shown in Fig. 5(b), depicting the location of the 1st order of VIPA light. Then we create a mask that controls both the 1st and 2nd order, with the output shown in Fig. 5(c). We can see the spectral dips have once again disappeared. The corresponding power distribution in Fig. 5(d), shows the location of the higher order light, which is above and below the main order, as expected.

4. Line-by-line pulse shaping results

Next we explore a series of line-by-line amplitude and phase shaping examples of GHz class frequency combs that showcase the programmable, broad bandwidth, and fine-resolution control of the shaper. We stress the programmable aspect here, because significant effort has been devoted to make the shaper act as a 'commercial type' device. To generate a mask, the user simply enters a desired phase and amplitude vector; the software then generates a mask which is sent to the SLM. The typical time to create a mask and have it applied on the SLM is on the order of 1-2 seconds, limited by the speed of the computer and the communication between the SLM driver and computer interface. This quick response allows this shaper to be used in feedback and optimization loops as we will show next.
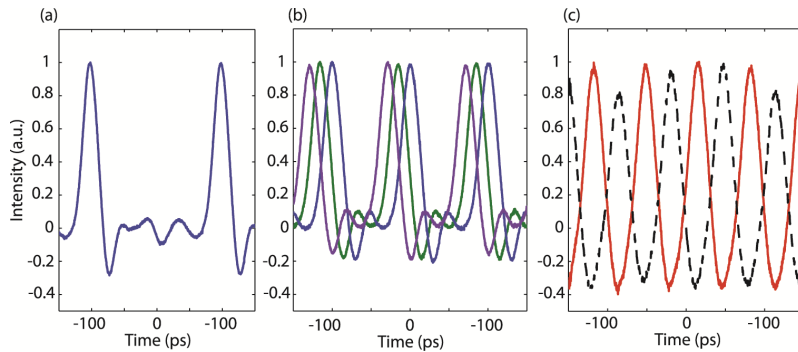
Fig. 6. (a) 200 ps pulse train with no mask applied, (b) (blue) 100 ps pulse train after amplitude-only mask was applied, doubling the repetition rate to 10 GHz, (green and purple) 100 ps pulse train time shifted by 15 and 30 ps, respectively (c) (black) 15 GHz tone after 3x Talbot mask, (red) 15 GHz tone after optimization program.

In our first experiment, we demonstrate control of an electro-optically generated frequency comb, comprised of 40 lines with 5 GHz spacing within 10 dB bandwidth. The inherent spectral phase of the comb was compensated for with 1.4 km of SMF fiber and spectrally broadened using a dispersion-decreasing-fiber soliton compressor [24], resulting in ~250 lines within 15 dB, and a pulse duration of ~2 ps full width at half maximum (FWHM). The pulse train was measured using a 22 GHz fast photodiode and monitored on a sampling oscilloscope, Fig. 6(a). We then create an amplitude and phase mask with the following properties. 1) We kill off every other line using amplitude shaping, resulting in a 10 GHz pulse train, Fig. 6(b) (blue). 2) We then apply linear phase ramps that shift the pulse by 15 and 30 ps Fig. 6(b) (green and purple respectively). Next we do a phase only shaping example that highlights an application for the programmability of the device. Starting with the initial 5 GHz comb, we create a phase only mask based on the Talbot effect, following a procedure used in [25], to triple the pulse repetition rate to 15 GHz, Fig. 6(c) (black). Due to slight imperfections in the driving voltage calibration of the shaper, the resultant pulse intensities are not uniform [25]. To correct for the variation we run an automated feedback program which compares the RMS value of the pulse heights and then slightly alters the phase values in the phase mask. After only 8 iterations, the deviation in pulse height decreases from 16% down to 3%, Fig. 6(c) (red). This programmatic control increases the ease-of-use of this state-of-art shaping apparatus, allowing for many applications. We have already demonstrated one such application in [26], where the shaper was used as part of a set-up to rapidly switch between optically generated RF waveforms. The broad bandwidth and fine resolution control allowed us to exert simultaneous, independent control of 4 separate 5 GHz frequency combs, each comprised of about 40 lines within 10 dB.

In order to highlight the accuracy of our simultaneous phase and amplitude control, we now take intensity cross correlation measurements. The source used here is a 10 GHz frequency comb comprised of 63 lines within −10 dB. The pulses are compressed to the bandwidth-limited duration (~1.5 ps) and split into two paths before the shaper. One path acts as a short pulse reference for the cross correlation measurement, the other goes through the shaper. Figure 7 gives the cross correlation measurements taken at the output of the shaper for (a) no mask applied, (b) a mask selecting every other spectral line while adding an additional 3rd order phase, (c) a zoom-in of one of the shaped pulses (blue). Trace (c) also shows the pulse intensity profile which was calculated using the measured optical spectrum and introducing the programmed phase profile. The intensity of traces (a) and (b) were normalized to compensate for a slight slope due to imperfect cross-correlator alignment over the full delay window. The zoom-in of one of the pulses in trace (c) shows close comparison between

calculated and measured pulse shape, and the long cubic tail serves as an example of our ability to arbitrarily control the phases of our pulses.
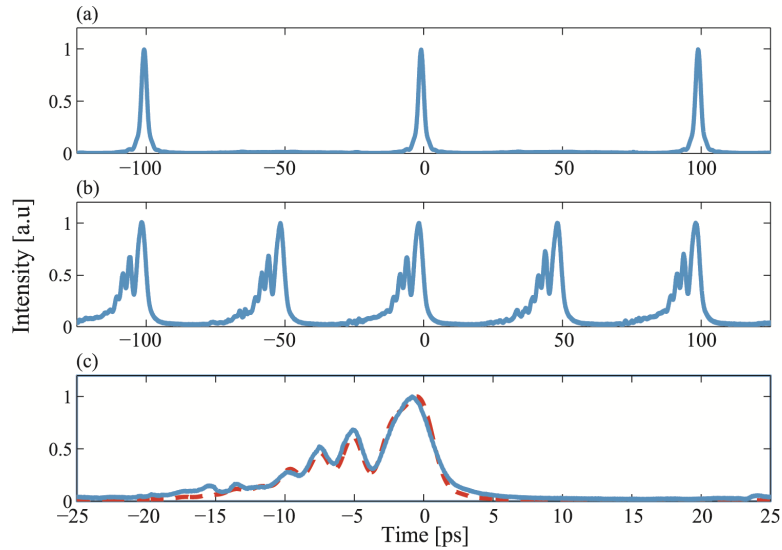

Fig. 7. Cross-correlation traces at the output of the shaper with a 10 GHz frequency comb input source (a), no mask applied, (b) mask applied which doubles the repetition rate by killing every other line and adds additional 3rd order phase, (c) zoom of single shaped waveform, measured (blue), simulated (red).
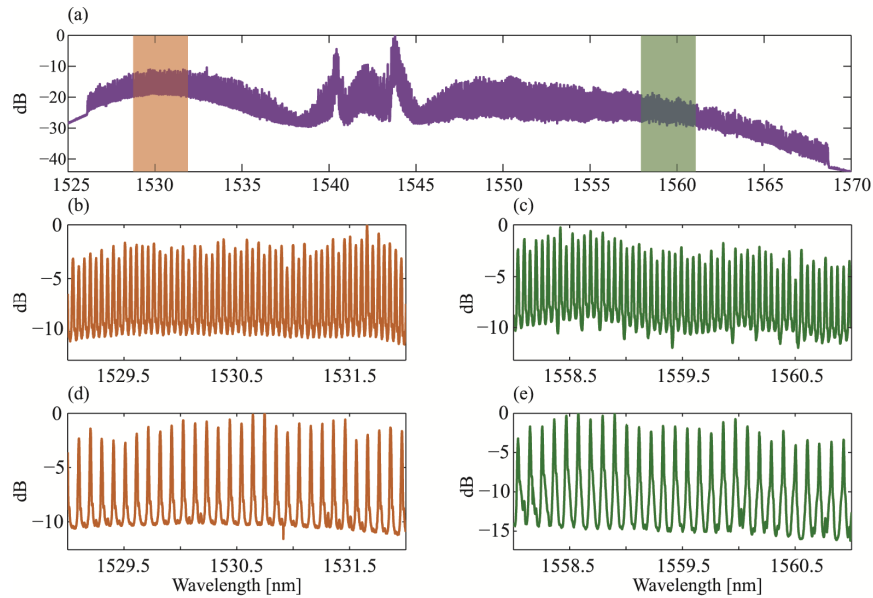

Fig. 8. (a) Spectrum of the non-linear broadened 6.5 GHz frequency comb (with a total of 836 lines) at the output of the shaper. Zoom of (b) orange and (c) green part of spectrum with no mask applied. Zoom of (d) orange (e) green part of spectrum with mask killing every other line.

To show broad-bandwidth operation and fine spectral control, we change the repetition rate of the comb to 6.5 GHz and spectrally broaden it by passing it though and Erbium Doped Fiber Amplifier (EDFA) followed by Highly Nonlinear Fiber (HNLF), leading to 836 lines spanning the C-band. We then create a mask killing off every other line. Figure 8 shows

spectral traces of the shaper output for (a) the full output spectrum of the shaper, (b)(c) zoomed portions of spectrum with no mask applied, (d)(e) zoomed portions of the spectrum with the mask applied. The masked spectral traces (d & e) exhibit good extinction ratio, suggesting the superpixels are correctly aligned across the full spectrum. To our knowledge the 836 comb teeth controlled independently here are the most yet reported in a line-by-line pulse shaping experiment. Furthermore, our achievable bandwidth (~C-Band) is limited currently by the availability of a flat optical source that we can use for our wavelength to spatial mapping procedure. In the experiments reported here, we use a ~40 nm ASE source which does not even use half of our available SLM pixels.

5. Conclusions

We have demonstrated a device that achieves programmable amplitude and phase control of finely spaced spectral features over a broad operation bandwidth. Our detailed wavelength to pixel mapping procedure addresses the nonlinear spacing of the VIPA diffracted light and allows for multiple order control. In addition, the programmability adds an ease-of-use that is comparable to current commercially available shapers. Experimental results of shaping multiple-GHz class frequency combs were provided which included line-by-line control of a record 836 comb lines.

Acknowledgments